Magnetic Phase Transition in a Nanonetwork of Solid ³He in Aerogel

D. I. Bradley,[*] S. N. Fisher, A. M. Guénault, R. P. Haley, N. Mulders,[†] G. R. Pickett, D. Potts, P. Skyba,[‡] J. Smith,
V. Tsepelin, and R. C. V. Whitehead

Department of Physics, Lancaster University, Lancaster, LA1 4YB, United Kingdom
(Received 31 March 2010; revised manuscript received 5 July 2010; published 16 September 2010)

When immersed in liquid ³He, the nanometer strands of aerogel are coated with a thin layer of solid ³He, forming a network of irregular nanotubes. Owing to its high purity and weak interactions, this system is ideal for studying fundamental processes. We report the first experiments on solid ³He in aerogel at ultralow temperatures, cooled by direct adiabatic demagnetization. Simultaneous nuclear magnetic susceptibility and heat capacity measurements indicate a magnetic phase transition.

The various phases of ³He at low temperatures have been studied extensively [1]. The extremely weak interatomic forces combined with almost absolute purity and the intrinsic nuclear spin of 1/2 make ³He particularly attractive for studying fundamental physics in condensed matter systems, although experiments are demanding owing to the small nuclear moment and the very low temperatures required. A great deal is known about liquid and solid ³He in the bulk, in reduced dimensions, and in restricted geometries [1–3]. It is therefore instructive to explore the physics of ³He in nanoscale geometries and to investigate emerging new phenomena.

The matrix of 98% silica aerogel is a very open network (98% free volume) of fine silica ''strands'' formed by the diffusion-limited aggregation of spherical silica particles forming a very irregular ''string of pearls'' [3], as shown schematically in Fig. 1. The particle diameters are of a few nm with a mean-free path between strands of ~100 nm [4]. When immersed in liquid ³He, the strands become covered by a ~1 nm layer of solid ³He atoms [5] thus forming a network of irregular nanotubes. For our experimental conditions (zero pressure), we expect the liquid within the aerogel surrounding the solid to remain normal at all temperatures [4–6], while *bulk* liquid ³He is a superfluid below 1 mK [1].

We have devised a new technique to cool the nanometer solid ³He layer to the lowest possible temperatures. The final cooling is by direct adiabatic demagnetization of the solid ³He, a process previously employed to cool bulk solid ³He [7]. We use a Lancaster-style nested-cell copper nuclear cooling stage [8], shown in Fig. 2. Following demagnetization of the copper, the superfluid ³He-*B* in the inner cell cools to ~100 μK as determined from the damping of vibrating wire resonators [9–11].

The experiments are made in a ³He filled ''black-body radiator'' [12] consisting of a sapphire tube containing 0.78 cm³ of superfluid as shown in Fig. 2. A small 0.23 mm diameter orifice at the top of the tube provides a weak thermal link to the main body of the inner cell. The superfluid in the tube cools to *T* ≈ 190 μK. In the following, the temperature *T* refers to that measured by a vibrat-

ing wire thermometer inside the top of the radiator tube. The wire thermometry is most sensitive and accurate at very low temperatures, below ~250 μK. The radiator contains a further vibrating wire used as a heater for calibration purposes. The temperature is limited by the weak thermal link and a heat leak of 3 pW arising from the slow release of heat from the walls of the radiator and the epoxy supports for the vibrating wires. Placed inside the radiator is a 3.7 mg 98% aerogel sample, in the form of two 1.5 mm thick slabs.

After the copper demagnetization, the magnetic field on the aerogel sample is *B* ≈ 20 mT. Using the small sample magnet shown in Fig. 2 the field is then increased to *B* ≈ 100 mT which warms the solid ³He and the surrounding superfluid to ≈400 μK. The system is then left to recool, typically reaching 200 μK overnight. The magnetic field on the sample is then reduced to the required final value over a period of a few minutes.

Figure 3 shows the evolution of the temperature *T* following aerogel demagnetizations to various final fields, preliminary measurements of this type were reported previously [13,14]. During demagnetization, *B/T* remains
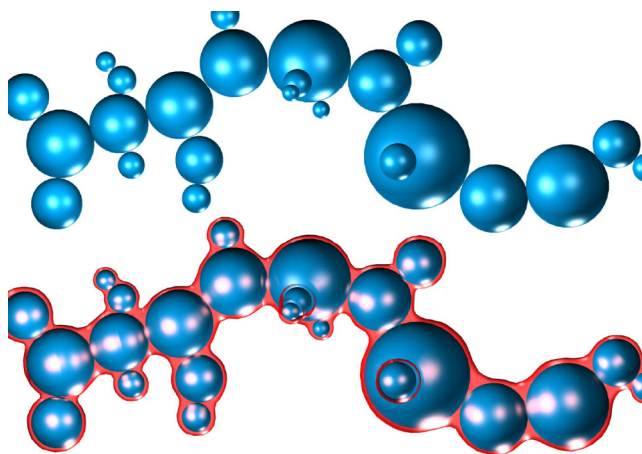

FIG. 1 (color online).   Schematic view of aerogel. Top: the bare string-of-pearls strands. Bottom: the strands coated with ~1 nm of solid when immersed in liquid ³He.
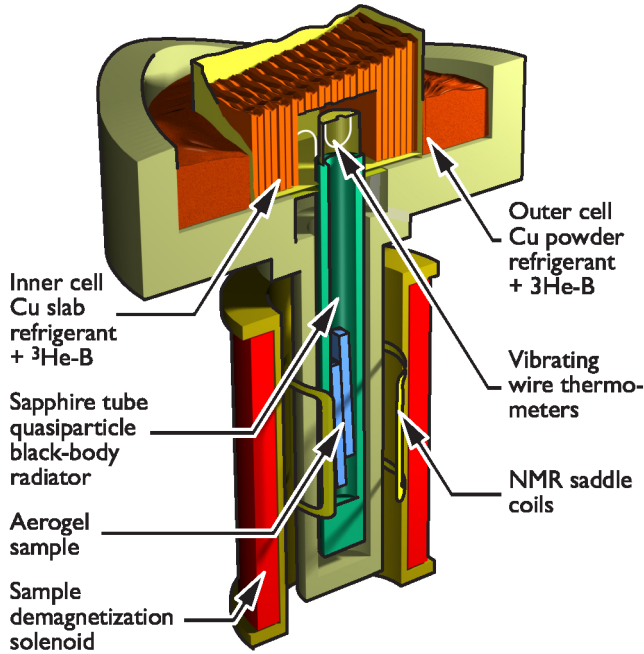
FIG. 2 (color online).   The experimental arrangement, see text.

Inner cell
Cu slab
refrigerant
+ ³He-B

Sapphire tube
quasiparticle
black-body
radiator

Aerogel
sample

Sample
demagnetization
solenoid

Outer cell
Cu powder
refrigerant
+ 3He-B

Vibrating
wire thermo-
meters

NMR saddle
coils

approximately constant down to $T \approx 130$ μK below which the solid decouples from the superfluid at the top of the radiator (see below), so the same lowest temperature of $T_{\min} \simeq 113$ μK is obtained regardless of the final field.

The normal liquid and solid helium inside the aerogel are in very good thermal contact and spin exchange between the confined liquid and solid phases is so rapid that their NMR signals are locked to give a single line [15]. From thermal conductivity measurements on similar aerogel samples [4,16,17] we infer that thermal gradients within the aerogel are negligible ($\Delta T \lesssim 0.3$ μK). Hence, the decoupling must arise from a temperature gradient between the top of the radiator and the aerogel sample, due to the ballistic heat transport. At the lowest temperatures immediately after the aerogel demagnetization, almost all of the heat leak into the radiator is absorbed by the aerogel sample with very little escaping through the radiator orifice. Quasiparticle excitations impinging on the aerogel are entangled by the strands and quickly thermalize. However, the finite flux of excitations needed to carry the heat gives rise to an effective thermal boundary resistance [18]. Further, owing to diffusive scattering at the cell walls, ballistic heat transport down the radiator tube requires an excitation density gradient and hence a temperature gradient. We have developed models which take these effects into account, but they depend on the precise geometry and on unknown quantities such as the diffusiveness of the walls [19]. Nevertheless, regardless of the precise parameters, the models clearly show that, owing to the very rapid fall of the excitation density with temperature in ³He-B, the temperature T measured at the top of the radiator very quickly decouples from the aerogel on cooling to low temperatures and the minimum temperature

$T_{\min} \simeq 113$ μK is independent of the solid ³He temperature T_s for $T_s \lesssim 100$ μK.

There are two clear features in Fig. 3. First, higher final fields result in a slower rate of warming at higher temperatures. This implies that the heat capacity of the solid ³He on the aerogel strands increases with increasing field at high temperatures as one would expect. Second, and of prime interest here, is the striking elbowlike feature observed in the warm-up curves at the lowest fields. Here, the initial warm-up rate slows very dramatically at $T \simeq 123$ μK, producing an almost constant temperature plateau lasting for several tens of minutes. At higher magnetic fields the plateau becomes less distinct and is no longer visible in fields above ~9 mT. A plateau corresponds to the absorption of heat at almost constant temperature, so in this region either the heat capacity is very large or there is a latent heat.

From the warm-up measurements of Fig. 3 we can calculate an effective heat capacity within the radiator. The power $\dot{Q}$ leaving the radiator is proportional to a thermometric variable called the width parameter W, which is inferred from the damping of the thermometer wire [12], $\dot{Q} = cW$. The radiator is calibrated, to find c, by applying a known power with the heater vibrating wire. The width parameter then provides an accurate absolute measure of the power leaving the radiator and the ambient heat leak is determined from the equilibrium (late time in Fig. 3) width parameter W_∞, i.e., $\dot{Q}_{\text{leak}} = cW_\infty$.

After demagnetization, the power leaving the radiator is less than the heat leak and the difference $Q_{\text{leak}} - \dot{Q}$ is absorbed by the warming solid ³He in the aerogel (the liquid heat capacity is negligible). The heat capacity of the solid is therefore given by $C_s = c[W(\infty) - W(t)]/\dot{T}_s$, where $\dot{T}_s$ is the rate of warming of the solid ³He. Since we cannot directly measure T_s, we instead use the measured
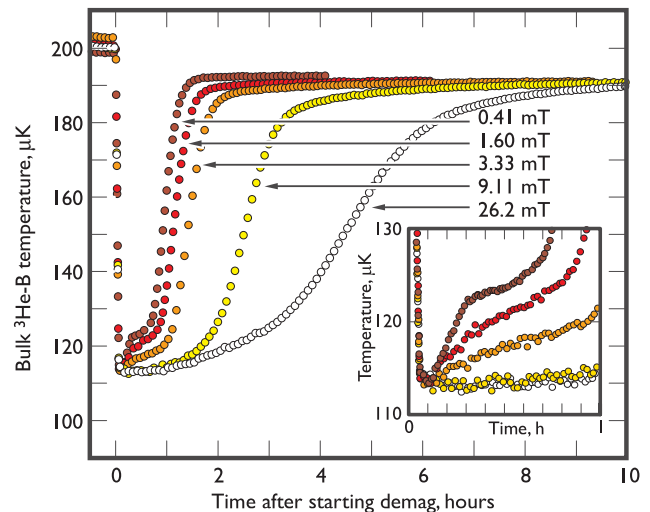

FIG. 3 (color online).   Temperature of the ³He-B inside the top of the radiator after demagnetizing the aerogel sample to various final fields. Inset shows further detail of the early-time behavior.

temperature T to define an effective heat capacity $C^* = c[W(\infty) - W(t)]/\dot{T}$.

In Fig. 4 we plot the effective heat capacity against T. At the higher temperatures, the heat capacity increases with applied field. At lower temperatures, a pronounced peak occurs for the lowest fields corresponding to the plateaus in Fig. 3. With increasing field this peak moves to lower temperatures until by ~ 9 mT, it is no longer visible. At temperatures above $T \sim 130$ μK, the aerogel-confined ^{3}He and surrounding bulk liquid are in good thermal contact so the solid ^{3}He and effective heat capacities are almost identical. At lower temperatures, the solid ^{3}He temperature T_s must be lower and increasing faster than the measured temperature T, so the effective heat capacity will overestimate the actual heat capacity. Thermal modeling, discussed above, indicates that the effects of thermal decoupling set in rapidly on cooling below $T \simeq 123$ μK, so the true solid ^{3}He heat capacity will have peaks which occur at slightly lower temperatures than those shown in Fig. 4, and it will fall much more rapidly at the very lowest temperatures.

We have further investigated the behavior by pulsed NMR measurements at 1.081 MHz in a magnetic field of 33.3 mT. The total magnetization of the system consists of contributions from (i) the solid ^{3}He spins; (ii) the normal ^{3}He inside the aerogel sample; (iii) the surrounding liquid ^{3}He in the radiator and (iv) liquid ^{3}He in the outer cell.

In Fig. 5 we show the magnetization, measured during a single warm-up taking 6 days, as a function of temperature after the aerogel was demagnetized to 33.3 mT. The magnetization was determined by integrating the free induction decay. Care was taken to ensure that the tipping pulses were sufficiently small to avoid significant heating. The solid signal dominates below ~ 10 mK. We find an excellent fit to the total magnetization of $M_T = A(1 - (\pi^2/12)(T/T_F)^2) + B/(T - \theta)$ above 1 mK, with a liquid Fermi temperature of $T_F = 322$ mK and a solid Curie-
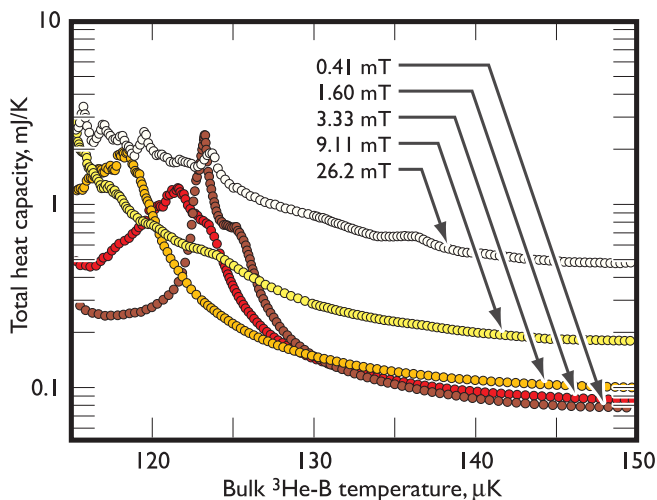
Weiss temperature of $\theta = 0.48$ mK consistent with other published data for zero pressure [5,15]. The Curie-Weiss law is only applicable at high temperatures: deviations occur as the magnetization approaches its saturation value. The slight wiggle in the data in the range 300–500 μK is most probably an artefact caused by uncertainties in the wire thermometry during the transition from ballistic to hydrodynamic behavior.

From the relative size of the Fermi-liquid and Curie-Weiss signals, we estimate the number of solid ^{3}He atoms to be $\sim 4 \times 10^{19}$, approximately 3% of the atoms inside the aerogel sample, comparable to measurements on similar samples [5]. From the fit to the solid contribution at high temperatures, the saturation magnetization, corresponding to full spin polarization of the solid, is expected to be $M_{sat} \sim 120$ in the units of Fig. 5. Thus the maximum magnetization observed corresponds to $\approx 75\%$ polarization.

The inset to Fig. 5 shows the magnetization M_T at the lowest temperatures. Two features stand out; first, for $T \lesssim 130$ μK the magnetization lies above the general trend of the data at higher temperatures. For these measurements, the heat leak after demagnetization was roughly twice larger than the measurements discussed earlier. Consequently the lowest measured temperature is a little higher, $T_{min} \simeq 126$ μK, and the modeling discussed above indicates that in this case thermal decoupling occurs rapidly below $T \simeq 131$ μK. The increase below ~ 130 μK can thus be attributed to decoupling. The green line in the inset shows a linear extrapolation of the data above 140 μK, where $T_s \simeq T$, to illustrate how the data might have looked, ignoring the down turn at the lowest temperatures (see below), if plotted against T_s.

FIG. 4 (color online).   The effective heat capacity at various magnetic fields as a function of the temperature T.
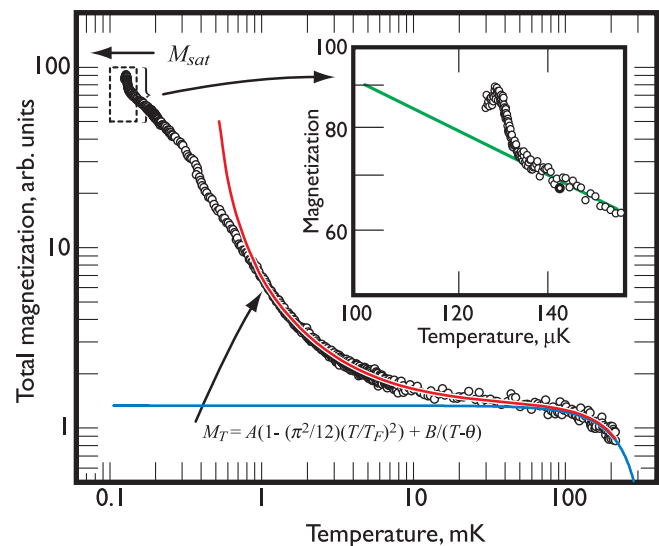

FIG. 5 (color online).   Total magnetization versus the temperature T. Blue line: fit to the normal Fermi-liquid contribution. Red line: fit to the liquid plus a Curie-Weiss solid above 1 mK. Inset shows the behavior at the lowest temperatures and a linear extrapolation (green line) of the higher temperature data.

The second feature revealed by the low-temperature data is the decrease in magnetization at the very lowest temperatures. The peak in the magnetization occurs several hours after the end of the aerogel demagnetization and there are no observable changes in the shape of the free induction decay during this period. Clearly it cannot be due to an initial cooling of the solid ^{3}He spin system since these spins constitute the refrigerant and must warm monotonically after demagnetization. The behavior suggests some form of antiferromagnetic ordering in the ^{3}He solid at the lowest temperatures. We cannot resolve a clear heat capacity peak at this relatively high magnetic field (see Fig. 4) but we note that magnetic ordering often displays different thermal and magnetic signatures [2].

Finally, we compare our measurements with other published results. Regarding the Weiss temperature, similar values ($\theta \simeq 0.5$ mK), have been reported previously for aerogel [5,15] and various other porous media and two-dimensional substrates [2]. The mechanisms responsible are not entirely understood, but are thought to arise from multiple-spin exchange within the solid and/or indirect spin exchange involving the fluid [2,20]. The low-temperature phase transition was quite unexpected. We are not aware of comparable behavior in other porous media. However there are similarities with bulk solid ^{3}He and with 2D solid ^{3}He films. The transition we observe in low fields is surprisingly sharp given that the aerogel surface must be very inhomogeneous. The behavior is consistent with a 1st-order transition with an associated latent heat. (The finite width of the transition might be interpreted as a narrow spread of transition temperatures due to the inhomogeneity.) Bulk solid bcc ^{3}He exhibits a 1st-order phase transition, at temperatures below ~ 1 mK and fields below ~ 400 mT, into an antiferromagnetic (U2D2) phase [1]. At the phase transition the entropy falls by $\sim 0.2 k_B$ per atom [21]. The transition we observe in aerogel occurs at roughly 10 times lower temperatures and fields. By integrating the heat capacity peak at low fields, $S = \int C/T dT$ we estimate that the entropy change per atom is $\sim 0.05 k_B$. A transition from a ferromagneticlike high-field phase to a low-field antiferromagnetic (V_2) phase has also been predicted [22], and possibly observed experimentally [23], for solid ^{3}He films in contact with bulk liquid. Our experiments may constitute the first observations of a similar ordering in a restricted nanoscale geometry.

In conclusion, we have performed the first measurements of solid ^{3}He in a nanonetwork at ultralow temperatures. We have developed a new technique to cool the system by direct adiabatic demagnetization. It is interesting to note that this technique also readily cools the adjacent normal liquid ^{3}He which can then be used to cool the surrounding bulk superfluid into a hitherto unexplored ultralow temperature regime. We have obtained very high spin polarizations and we have observed thermal and magnetic anomalies which indicate that a phase transition,

possibly to an antiferromagnetic phase, occurs at temperatures below 130 μK and in low magnetic fields. Our observations show similarities to both the bulk solid and to solid ^{3}He films which suggests that antiferromagnetic ordering may be a widespread feature of these systems, common also to nanoscale structures. Further work is required to better quantify the phase transition. It would be interesting to extend the magnetization data to lower fields and to improve the thermal coupling to infer lower solid ^{3}He temperatures. The current experimental cell was limited to low pressure experiments. However the thickness of the solid ^{3}He layer increases by a factor of order two with increasing pressure [5], so the pressure dependence will reveal important information on how the magnetic ordering depends on the nanometer thickness of the ^{3}He layer.

*I.Bradley@Lancaster.ac.uk
†Present address: Department of Physics and Astronomy, University of Delaware, Newark, DE, USA.
‡Present address: Inst. of Exp. Physics, Slovak Academy of Sciences, Watsonova 47, 04001 Košice, Slovakia.

[1] E. R. Dobbs, *Helium Three* (Oxford University Press, Oxford, 2000), and references therein.
[2] H. Godfrin and R. E. Rapp, Adv. Phys. **44**, 113 (1995), and references therein.
[3] W. P. Halperin, H. Choi, J. P. Davis, and J. Pollanen, J. Phys. Soc. Jpn. **77**, 111002 (2008).
[4] S. N. Fisher *et al.*, Phys. Rev. Lett. **91**, 105303 (2003).
[5] J. A. Sauls, Yu. M. Bunkov, E. Collin, H. Godfrin, and P. Sharma, Phys. Rev. B **72**, 024507 (2005).
[6] J. V. Porto and J. M. Parpia, Phys. Rev. B **59**, 14 583 (1999).
[7] T. Lang *et al.*, Phys. Rev. Lett. **77**, 322 (1996).
[8] G. R. Pickett and S. N. Fisher, Physica (Amsterdam) **329-333B**, 75 (2003).
[9] S. N. Fisher *et al.*, Phys. Rev. Lett. **63**, 2566 (1989).
[10] S. N. Fisher *et al.*, J. Low Temp. Phys. **83**, 225 (1991).
[11] C. Bäuerle *et al.*, Phys. Rev. B **57**, 14 381 (1998).
[12] S. N. Fisher *et al.*, Phys. Rev. Lett. **69**, 1073 (1992).
[13] D. I. Bradley *et al.*, J. Low Temp. Phys. **138**, 129 (2005).
[14] D. I. Bradley *et al.*, Low Temp. Phys. **850**, 243 (2006).
[15] D. T. Sprague *et al.*, Phys. Rev. Lett. **75**, 661 (1995).
[16] S. N. Fisher *et al.*, J. Low Temp. Phys. **126**, 673 (2002).
[17] P. A. Reeves *et al.*, J. Low Temp. Phys. **129**, 185 (2002).
[18] S. N. Fisher *et al.*, Physica (Amsterdam) **329–333B**, 311 (2003).
[19] D. I. Bradley *et al.*, Low Temp. Phys. **850**, 93 (2006).
[20] A. Schuhl *et al.*, Phys. Rev. B **36**, 6811 (1987).
[21] W. P. Halperin *et al.*, Phys. Rev. Lett. **32**, 927 (1974).
[22] S. Tasaki, Prog. Theor. Phys. **82**, 1032 (1989).
[23] L. J. Friedman *et al.*, Phys. Rev. Lett. **57**, 2943 (1986).